Journal Pre-proofs

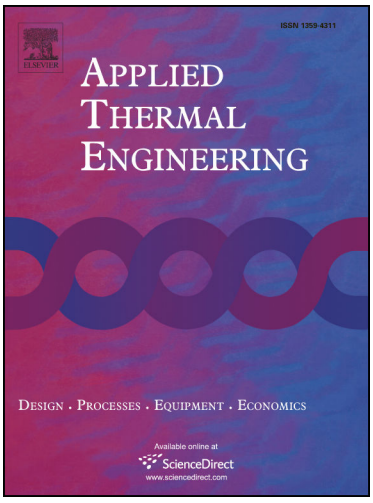

Impact of Reactor Design on the Thermal Energy Storage of Thermochemical Materials

A.A. Hawwash, Hamdy Hassan, Khalid El feky

PII: S1359-4311(19)34627-7
DOI: https://doi.org/10.1016/j.applthermaleng.2019.114776
Reference: ATE 114776

To appear in: *Applied Thermal Engineering*

Received Date: 5 July 2019
Revised Date: 3 December 2019
Accepted Date: 5 December 2019

Please cite this article as: A.A. Hawwash, H. Hassan, K.E. feky, Impact of Reactor Design on the Thermal Energy Storage of Thermochemical Materials, *Applied Thermal Engineering* (2019), doi: https://doi.org/10.1016/j.applthermaleng.2019.114776

Impact of Reactor Design on the Thermal Energy Storage of Thermochemical Materials

A.A. Hawwash[1,2], Hamdy Hassan[1,3*], Khalid El feky[1]

[1]Energy Resources Engineering Department, Egypt- Japan University of Science and Technology, Alexandria, Egypt
[2]Mechanical Engineering Department, Benha Faculty of Engineering, Benha University, Benha, Egypt.
[3]Mechanical Engineering Department, Faculty of Engineering, Assiut University, Assiut, Egypt.
hamdy.aboali@ejust.edu.eg, ahmed.hawwash@ejust.edu.eg
Corresponding authors:
Hamdy Hassan
hamdyaboali@yahoo.com

Abstract

This work presents the impact of reactor design on the thermal performance and energy storage during the dehydration of salt hydrate of thermochemical material; magnesium chloride hexahydrate ($MgCl_2.6H_2O$). The dehydration process is performed by flowing hot air through the material. A transient 2D axisymmetric mathematical model for an open thermochemical long-term heat storage reactor by using COMSOL Multiphysics software is presented. Two configurations of the reactor design are considered; cylinder and truncated cone having the same height and volume of seven designs; cylindrical (base design), convergent truncated cones of inlet to outlet area ratio (AR) 1.4, 4 and 5.8 and divergent truncated cones of AR 0.71, 0.25 and 0.17. Results show that the reactor of lower AR has the lower charging time and higher pressure drop and temperature difference. However, the reactor design hasn't great impact on the maximum value of water content concentration inside the thermochemical material. Maximum variation of the energy storage of the thermochemical material is about 25.5% and the dehydration time more than three times due to design reactor changing. Maximum stored energy is achieved for the reactor truncated cone of AR 1.4 while the minimum desorption time is obtained for the cone of AR 0.17%.

Keywords*:* Thermochemical energy storage; Reactor design; Salt-hydrates; Magnesium Chloride hexahydrates; Concentration; Energy Storage

Nomenclature

a	Reactor radius at the inlet side, m	w	Width of the bed, m
b	Reactor radius at outlet side, m	**Greek symbols**	
C	Specific heat, J/kg.K	E	Material porosity
C_f	Dimensionless form-drag constant	ρ_s	Solid density, kg/m^3
C_p	Specific heat at constant pressure, J/kg.K	ρ_f	Fluid density, kg/m^3
d_e	Equivalent diameter, m	ρ_b	Bulk density, kg/m^3
d_p	Particle diameter, m	μ	Dynamic viscosity, Pa.s
D_w	Water- air diffusivity	ξ_w	Water vapor mass fraction
E_a	Activation energy, J/mol	Ɛ	Void fraction of the bed
h	Reactor height, m	τ	Overall reaction time, s
ΔH	Heat of the reaction, J/kg	**Abbreviations**	
HR	Relative humidity	amb	Ambient
K	Specific permeability, m^2	AR	Area Ratio
K_{ins}	Insulation thermal conductivity, W/m.K	da	Dried air
K_m	Porous material thermal Conductivity, W/m.K	2D	Two dimensions
m_{da}	Dry air mass, g	eq	Equilibrium
m_w	Vapor mass, g	F	Fluid
P	Partial pressure, pa	G	Reactive gas
∇P	Pressure drop, pa	in	Inlet
P_{eq}	Equivalent pressure, pa	ins	Insulation
P_f	Fluid pressure, pa	LHS	Latent Heat Storage
$\dot{q}'''$	Heat source rate per unit volume, W/m^3	m	Mass, kg
Re	Reynolds number	M	Mean
r_w	Water absorption reaction rate, kg Water/m^3.s	out	Outlet

r_p	Particle size	S	Solid
t	Time, s	S_0	Dehydrated material
T_f	Fluid temperature, °C	S_1	Hydrated material
T_s	Salt material temperature, °C	SHS	Sensible Heat Storage
T_{in}	Inlet air temperature for the reactor, K	WS	Water saturated
T_{amb}	Ambient air temperature, K	W	Water vapor
u	Darcy velocity, m/s	TCM	Thermochemical Material
v	Inlet air velocity for the reactor, m/s	THS	Thermochemical Heat Storage

1. Introduction

Since the energy crises and due to the limited fossil fuel sources and the global warming phenomena because of using fossil fuels, renewable and sustainable energy have been widely utilized as a promising alternative solution. Overall, 25% of total energy consumption is related to buildings demand and in the developing countries, the building sector accounts for around 40-50% of the consumed energy [1–3]. Furthermore, half of the consumption energy in the building is directed to space heating and hot domestic water in winter [4]. However, solar energy is the most promising resource in the renewable energy section, however, the weakness of collected solar radiation over the winter is the most challenge for this great energy [5]. This requires using an efficient technique to store solar energy for a long period in order to utilize this heat at winter period. Thus many researchers are recently interested and pay their attention for promising long-term solar heat storage [6–8] to reuse a large scale of solar energy and achieve efficient energy storage. The Latent Heat Storage (LHS), Sensible Heat Storage (SHS) and Thermochemical Heat Storage (THS) are main types of thermal energy storage [9]. Compared with sensible and latent heat storage, THS has the highest energy density of about 200-500 kWh m^{-3} [10] and exhibits an ignored heat loss during the storage period because the energy is stored in a chemical potential [7].

Generally, the thermochemical reactions with chemisorption or without sorption are the main two types of THS [11,12]. The second type is a reversible exothermic reaction that occurs between two or more distinct thermochemical substances, where a great amount of heat energy is generated or stored. Additionally, the process reaction progression is complicated process to obtain the byproduct [13–19]. During the thermochemical storage process, a reversible reaction takes place during hydration and dehydration for the thermochemical material (TCM) in specific conditions,

which is exo/endothermic chemical reaction. This means that TCM stores and releases thermal energy via charging/hydration chemical reaction [20]. Figure 1 shows the main steps of the charging and hydration processes of the thermochemical energy storage. During summertime, while the hot air is the outlet of the solar collector or waste heat passes into adsorbent (TCM inside the reactor), the charging (desorption or dehydration) process takes place as soon as the vapor is removed from the adsorbent and transferred to the outlet air. During winter season, hydration (adsorption or discharging) process takes place when the vapor (adsorbate) passes through the porous material (adsorbent) leading to a production of the hot outlet air.

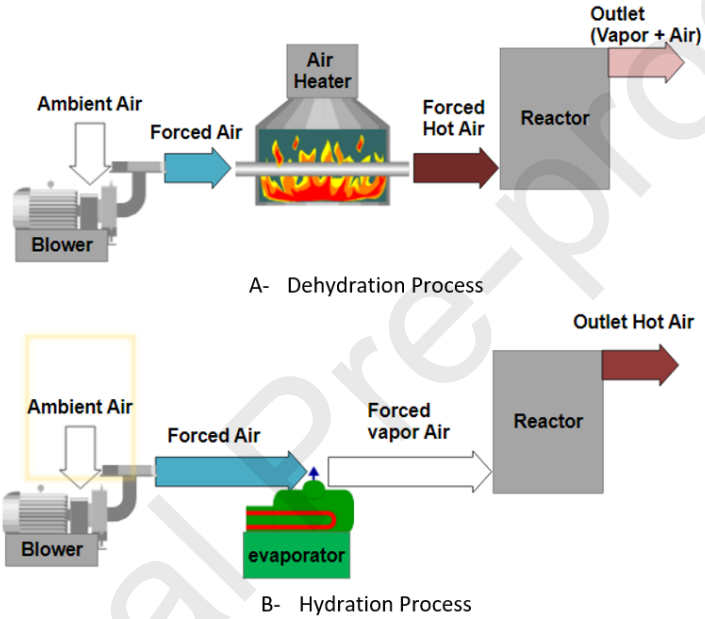

Figure 1: Main steps for the reversible reaction in an open thermochemical storage system.

Thermochemical reactions used for heat recuperation are recently facilitated by using salt hydrates [20]. When salt hydrates are exposed to waste energy or energy gained via solar collectors during summer months, they will be charged and produce vapor. Then, the products are stored until cooler weather, or at a desirable time, the required sensible heat is released from the salt in a hydration process. Selecting and screening salt hydrate depend on corrosiveness, operating pressure, sustainability, recyclability, environmental safety, toxicity, material cost, energy density, charging and discharging temperature range, and stability. THS systems can apply both chemical reactions and sorption to produce heat economically and efficiently. Recently, sorption thermal energy storage becomes a promising choice for solar thermal heat storage [21] because of its high relatively heat storage capacity and its ability to preserve energy for longer periods with limited heat loss. While the thermochemical materials (TCMs) have advantages, they have challenges

where the recyclability of TCMs is significantly low, their rate of heat and mass transfer is relatively low and during hydration, a formation of layer like gel may be formed. Aydin et al. [22] and Donkers [23] found that the stored energy density for TCM, latent and water storage are about 100–500 kWh/m^3, 90 kWh/m^3 and 54 kWh/m^3, respectively for storing 6.7 MJ of energy. Moreover, the required stored volume is 1 m^3, 10 m^3, 20 m^3 and 34 m^3 for TCM, sorption, latent, and water storage, respectively.

Different studies related to long term thermal heat storage by using TCM have been presented. Zondag et al. [24] examined experimentally magnesium chloride hexahydrate ($MgCl_2.6H_2O$) in open and closed thermochemical storage systems for both hydration and dehydration process. During hydration, a gel-like structure layer was formed beside the evaporator due to over-hydration in closed and open system. In consequence, pressure drop inside the reactor was raised significantly compared with other hydration tests. Hence, a carrier material was used to avoid the layer gel formation during hydration. It was concluded that, at a heating rate 1°C, the charging of magnesium chloride hexahydrate started at 50 °C and the monohydrate was formed at 120 °C. In the evacuated closed system, the reactor temperature reached 85 °C at 32 mbar vapor pressure (the temperature of the evaporator was 25 °C). Moreover, the sorption bed temperature increased from 50 to 70 °C at 12 mbar vapor pressure where the temperature of the evaporator was 10 °C and the initial reactor temperature was 50 °C. Additionally, during dehydration, since the inlet air temperature reached 135 °C, hydrogen chloride gas (HCl) was detected inside the reactor. The feasibility of an open thermochemical system was studied experimentally by Marias et al. [25] for both complete hydration and charging process under realistic conditions during theoretical assumption and the energy balance for hydration and dehydration process. They found that when the inlet temperature of the ambient air was 65 °C during dehydration, the temperature and absolute humidity of the inlet air were 15 °C and 7-8, respectively. When aluminum potassium sulfate 12-hydrate ($KAl(SO_4)_2.12H_2O$) was selected as thermochemical material, the moist air was used as a reactive during the hydration process. Additionally, they concluded that the layer formation like gel could be avoided by changing the area to length ratio of the reactor. Furthermore, the pressure drop inside the reactor increased and decreased during discharging and charging processes, respectively. Rubino and Boer [26] developed a mathematical model for an open atmospheric thermo-chemical reactor using COMSOL Multiphysics Software to solve the proposed system of the algebraic and partial differential equations in both time and space. They concluded that this

model could be used to investigate more operation conditions for both hydration and dehydration processes in the reactor. Furthermore, the model could be utilized for examining the effects of reactor design on the heat storage efficiency during dehydration. Marias et al. [27] carried out an experimental work on open-air thermochemical storage by using two porous materials; Strontium bromide mono/hexahydrate and Aluminum potassium sulfate 3-12 hydrate. Moreover, they built a theoretical model to predict the outlet air conditions when the inlet air conditions are known besides their study of charging and hydration processes. They defined charging-hydration operating line and they concluded that the reactor performance or reaction effectiveness depends on the thermochemical material type whereas it equals 0.8/0.9 and 0.5/0.6 for strontium bromide/ water pairs and potassium alum/water pairs, respectively. Lele et al. [28] investigated the impact of a helical coil and plate-fin heat exchangers embedded in a magnesium chloride hexahydrate closed reactor on its performance. They built their model based on finite element method using COMSOL Multiphysics Software. They found that the contact layer between the material bed and the heat exchanger is inefficient. In addition, the agglomeration that arose during hydration reduced the heat transfer rate as the vapor transportation into the bed decreases. Moreover, the fin-plate heat exchanger was the most appropriate related to the pressure drop and the temperature variation. Moreover, Lele et al. [29] built a mathematical model for the heat and mass transfer for the thermal decomposition process (dehydration) in the closed thermochemical heat storage system. The model is based on partial differential equations (PDEs) of the energy, mass and conversion in the reactor. They studied the dehydration dynamics and temperature distribution for the reactor. They presented the model based on limited assumptions and their model can predict the behavior of the thermal and mass transport. A closed thermochemical heat storage system with different heat exchangers (honeycomb) was proposed by Lele et al. [30] to avoid some challenges like agglomeration and gel-layer formation at the beginning of the reactor. They investigated a pure strontium bromide as an absorbent for dehydration and hydration. The charging process was at temperature 105 °C and the hydration process was at vapor pressure of 42 mbar. Their conclusion illustrated that the cycling stability of $SrBr_2.6H_2O$ can be reached. Lele et al. [31] created a 2D symmetric model for a closed thermochemical heat storage system with heat exchanger based on $MgCl_2.6H_2O$ as TCM by using COMSOL Multiphysics Software. They focused on the synthesis (hydration) process since it is a challenge to release heat suited for heat space applications. Moreover, a sensitivity study for a heat exchanger design was evolved to

increase the released temperature during discharging. The water vapor concentration was fixed at 500 $mol.m^{-3}$, and the pressure was around 1230 Pa. The plate size and distance between plates in the heat exchanger were optimized to improve the mass transfer. Also, the bed temperature profile and the velocity inside the reactor were investigated numerically. Their numerical results exhibited that the reaction temperature has an impact on the reaction conversion than the pressure. Furthermore, the mass flow rate lower than 0.001 $kg.h^{-1}$ is important to reach quasi-complete hydration with 4 to 5 cm bed thickness. The optimal porosity of the thermochemical material was found around 0.71 from the mass and heat transfer dilemma analysis views. The performance of the thermochemical composite sorption storage system (TCSSS) was examined theoretically by Yan et al. [32] by utilizing $MnCl_2$-$SrCl_2$-NH_3 . Their results revealed that TCSSS cycle is effective for integrating energy storage and energy upgrade of low-grade thermal energy. Besides, thermal energy temperature can be raised from 81 to 170 °C by TCSSS cycle.

Despite that, the literature presented different research works related to long-term heat storage utilizing TCM, but to the authors' best survey, there is no previously published work on the impact of the bed reactor design on the dehydration process of the THS. In this work, a theoretical transient study on the impact of two configurations of the reactor design; cylindrical and conical on the dehydration process is carried out for the thermochemical material of magnesium chloride hexahydrate which was not studied before. Seven area ratios (inlet area to outlet area (AR)) of the reactor having the same volume and length are considered which are; cylindrical (case 1, base case), truncated cones (convergent cone) of AR 1.4, 4 and 5.8 and truncated cones (divergent cone) of AR 0.71, 0.25 and 0.17. The dehydration process is carried out by flowing air through the thermochemical material. A complete 2D axisymmetric transient model is built for the reactor including the airflow and the dehydration process of the thermochemical material by using commercial software (COMSOL Multiphysics Modeling Software). The model is validated by using experimental results. Hence, the best design for the reactor is defined based on the comparison between the different reactor designs. The impact of the reactor design on the dehydration rate, dehydration process, air temperature difference and pressure drop through the reactor, concentration of the vapor inside the outlet air and the stored energy inside the salt hydrate is considered which was not considered before.

2. Geometry and Model Implementation

In this work, to study the impact of the reactor design on the dehydration process, two shapes of the reactor (cylindrical and conical) are examined and investigated numerically at different sizes for TCM material; $MgCl_2.6H_2O$. This material is selected because the range of operating temperatures for the hydration and dehydration is appropriate with domestic applications and solar collector systems (evacuated tube and flat plate solar collectors)[33,34]. The reactor designs have a significant change in the geometry entrance and outlet area without any change in the height and volume of the thermochemical reactor. For all studied cases, the height and volume of the reactor are considered constant at 22 cm and 20 litters, respectively. Seven cases of the reactor design are considered in this study as stated in

Table 1; cylindrical shape (case 1), truncated cone where the outlet area is lower than the inlet area of three different dimensions (cases 2, 3, and 4), and truncated cone with the greatest area at the inlet of three different dimensions (cases 5, 6, and 7). The main change in the truncated cone design is the inlet and outlet area. In consequence, these different reactor designs are examined as an open thermochemical system. Figure 2 indicates the schematic diagram of the first design (case 1), which is the cylindrical reactor with its dimensions. Moreover, the operating conditions used in this study are also stated in figure 1. As a result of the reactor design configuration, the model geometry of the studied reactor, the reactor model is considered a 2D axisymmetric.

2.1 Mathematical Model

An open thermochemical heat storage system is selected to be simulated because of its simplicity and cheapness compared to the closed evacuated system [10]. During desorption dehydration, since the hot air passes via the porous materials, the dehydration is defined as an endothermic reaction which takes place when the totally hydrated porous material is exposed to hot gases stream. Air and solid material have the same temperature as a pseudo-homogeneous medium, and only the solid heat capacity is assumed in the energy balance.

Table 1: Dimensions of the studied designs of the reactor.

	Case 1	Case 2	Case 3	Case 4	Case 5	Case 6	Case 7
a: inlet (cm)	17	18.4	20.949	22	15.5	10.47	9.125

b: outlet (cm)	17	15.5	10.47	9.125	18.4	20.949	22
AR (ratio of inlet to outlet area)	1	1.4	4	5.8	0.71	0.25	0.17
Height (h) = 22 cm Volume= 20 litters	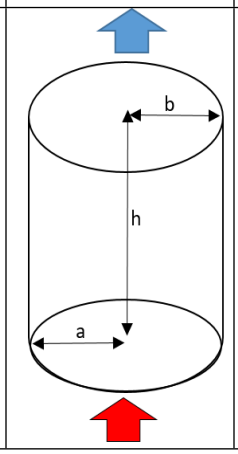	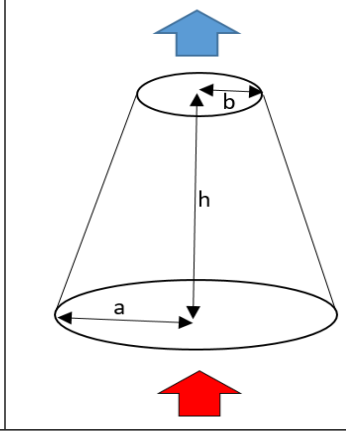			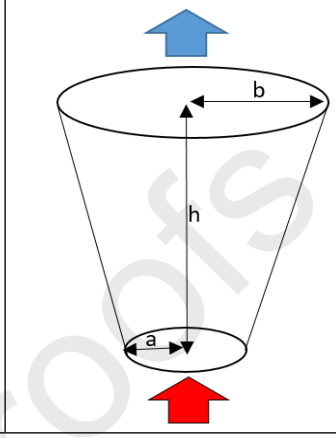		

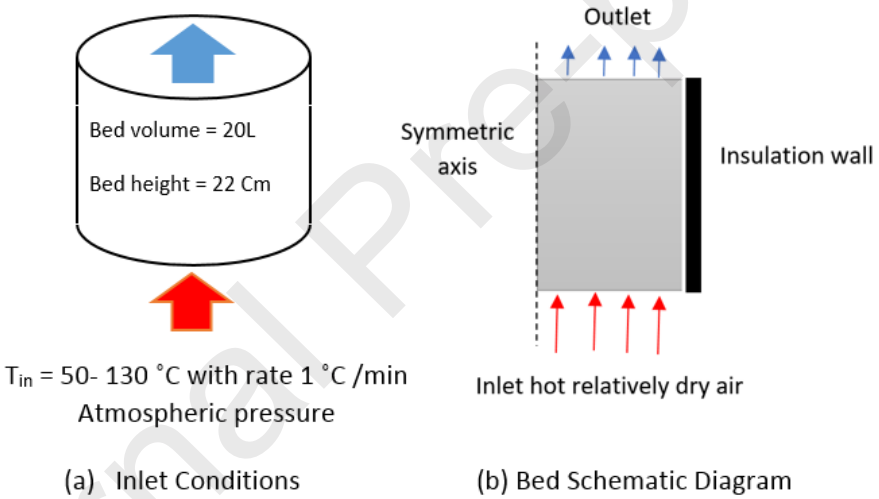

Figure 2: Model inlet conditions and Bed schematic diagram.

To model the hydration and dehydration process through the reactor, all physical parameters are assumed constant during the reaction and there is no diffusivity between the gas and solid. Moreover, the friction in the energy balance is equal zero, the mass transfer resistance on the airside is negligible, and Darcy's law is used to define pressure drop via the porous media. Additionally, the gas velocity is kept constant and the heat transfer by natural convective and radiation is negligible. Olives and Mauran [35] concluded that thermal radiation is not considered when the operating temperature ranges from 10 to 90 °C for any thermochemical heat storage

system. Furthermore, the main heat transfer takes place by conduction for these systems which have water vapor, according to the Fourier law.

The reaction between the vapor and the salt is complete and instantaneous. Therefore, there is no convection heat transfer between the vapor and the salat. Mass transfer depends on velocity and vapor pressure at the boundaries of the porous media. In our case, Brinkman equation is applied since the airflow through the porous material is laminar, as the Reynolds number is lower than 10 in the packed bed. It means that the mass transfer is controlled by Brinkman equation and the total pressure inside the reactor is the vapor pressure which depends on the evaporator temperature. Table 2 presents the properties and parameters used in the present numerical simulation [26].

Table 2: Material properties and operating conditions used in the numerical simulation.

Parameter	K (m^2)	ε	K_{ins} (W/m.K)	K_m (W/m.K)	ρ_b (kg/m^3)	T_{amb} (°C)	v (m/s)	D_w	E (J/mol)
Value	4.48e-9	0.7	0.05	0.704	850	25	0.1	2.6e-5	70400

2.1.1 Reaction Equations

The general equation of the nonvariant reversible reaction between the gas and solid is given by [6,31,36,37]:

$$Salt.xH_2O_{(s)} + Heat \leftrightarrow Salt.(x-y)H_2O_{(s)} + yH_2O_{(g)} \quad (1)$$

$$S_0 + \nu G \leftrightarrow S_1 + \Delta h_r^0 \quad (2)$$

The reversible thermochemical reactions for $MgCl_2.6H_2O$/water reactive pair are expressed as following[25,26,29,31,38–43]:

$$Mgcl_2.6H_2O \Leftrightarrow MgCl_2.4H_2O + 2H_2O \quad (3)$$

$$Mgcl_2.4H_2O \Leftrightarrow MgCl_2.2H_2O + 2H_2O \quad (4)$$

where, $MgCl_2.6H_2O$ and $MgCl_2.4H_2O$ represent the hydrated (S_1) and dehydrated (S_0), respectively in equation 2 and $MgCl_2.4H_2O$ and $MgCl_2.2H_2O$ are the hydrated (S_1) and dehydrated (S_0), respectively in equation 3.

2.1.2 Mass Balance

During the dehydration, the fully hydrated sample of $MgCl_2$-$6H_2O$ is exposed to relatively dry and hot air stream. On the microscopic scale, the pores distribution in the porous medium is irregular and the flow measurements (pressure, velocity, etc.) will be irregular. Due to this flow, the heat spreads into porous media. Thus, the temperature of the grain increases by diffusion and

endothermic dehydration reaction initiates. In consequence, the vapor releases and diffuses into holes, and the mass fraction of water vapor varies through the porous material during the dehydration process. The vapor is transferred from the porous material by cooled air stream [44]. So, it is expected that the cone shape of the reactor will affect the dehydration process. The mass conservation equations for water vapor and solid materials are expressed as [26];

$$\varepsilon\rho_f \frac{\partial \xi}{\partial t} + \rho_F (u.\nabla)\xi_w = r_w \tag{5}$$

$$(1-\varepsilon)\frac{\partial \rho_s}{\partial t} = -r_w \tag{6}$$

where, the water vapor mass fraction $\xi_w = \frac{m_w}{m_w + m_{da}}$, and m_w, m_{da}, r_w, u, ρ_s, ρ_f and ε are vapor mass, dry air mass, water absorption reaction rate, Darcy velocity vector, solid density, fluid density, and void fraction of the bed, respectively.

2.1.3 Momentum Balance

For the porous material, Darcy law governs the momentum conservation only when the velocity is low to achieve this condition $R_e < 1$[26]. However, Darcy equation computes only the pressure, and the fluid velocity is described by the fluid viscosity, pressure gradient, and permeability. At high velocity and Re >1 inside the laminar regime, Brinkman's equation is reliable instead of Darcy's equation [45]. Brinkman's equation is considered an extension to Darcy low as it obtains a relation between the porosity and permeability of the porous material which is valid only when the material porosity is higher than 0.6 [45]. Although, in a laminar flow regime, Brinkman's equation is considered for computing pressure fields and fluid velocity of the single-phase flow inside the porous material. Then, Brinkman's equations interface is used in the model [46];

$$\rho\frac{\partial u}{\partial t} = \nabla\left[-PI + \mu\frac{1}{\varepsilon_p}(\nabla u) - \frac{2}{3}\mu\frac{1}{\varepsilon_p}(\nabla u)I\right] - \left(\mu k^{-1} + B_f|u| + \frac{Q_{br}}{\varepsilon_p^2}\right)u \tag{7}$$

2.1.4 Energy Balance

The energy balance for the solid is computed from [26];

$$(1-\varepsilon)\rho_s C_s \frac{\partial T_s}{\partial t} = (1-\varepsilon)k_s\nabla^2 T_s + q_s''' \tag{8}$$

For the fluid, the energy balance equation is expressed by [26];

$$\varepsilon\rho_F C_{pF}\frac{\partial T_F}{\partial t} + \rho_F C_{pF} u.\nabla T_F = \varepsilon k_s \nabla^2 T_s \tag{9}$$

The thermal equilibrium between the gas phase and solid leads to assuming $T_s = T_f = T$, and from equations (8) and (9), it is found that [26];

$$(\rho C)_m \frac{\partial T}{\partial t} + (\rho C)_F (u.\nabla)T = k_m \nabla^2 T + q_s''' \quad (10)$$

where

$$(\rho C)_m = (1-\varepsilon)(\rho C)_s + \varepsilon (\rho C_p)_F \quad (11)$$

$$k_m = (1-\varepsilon)k_s + \varepsilon k_F \quad (12)$$

In these equations, C, $C_{p,}$ and $\acute{q}$ are specific heat, specific heat at constant pressure and heat source rate per unit volume. The reactor heat source is expressed by [26];

$$q_s''' = \Delta H.r_w \quad (13)$$

where ΔH and r_w are the salt material heat of reaction and the rate of reaction for uptake water, respectively. The Equilibrium curve and the relationship between the vapor pressure, temperature, and water vapor for $MgCl_2$-$6H_2O$ are shown in Figure 3 [26]. They show a graph of the equilibrium pressure for the different dehydration steps in two porous materials as a function of the temperature. On one hand, for magnesium chloride hexahydrate, the safe full dehydration reaction takes place in two steps, as it loses two molecules of water in the first step, results in decreasing and increasing in $Mgcl_2.6H_2O$ and $Mgcl_2.4H_2O$ concentration, respectively at inlet air temperature less than 70 °C. In a similar way in the second step, when the inlet air temperature rises from 105 to 120 °C, the concentration of $Mgcl_2.4H_2O$ begins to decrease compared with the rising in $Mgcl_2.2H_2O$ concentration because of losing two vapor molecules. As soon as the temperature reaches 130 °C, the undesired HCl gas appears in the output mixture results in significant corrosion in the system [26].

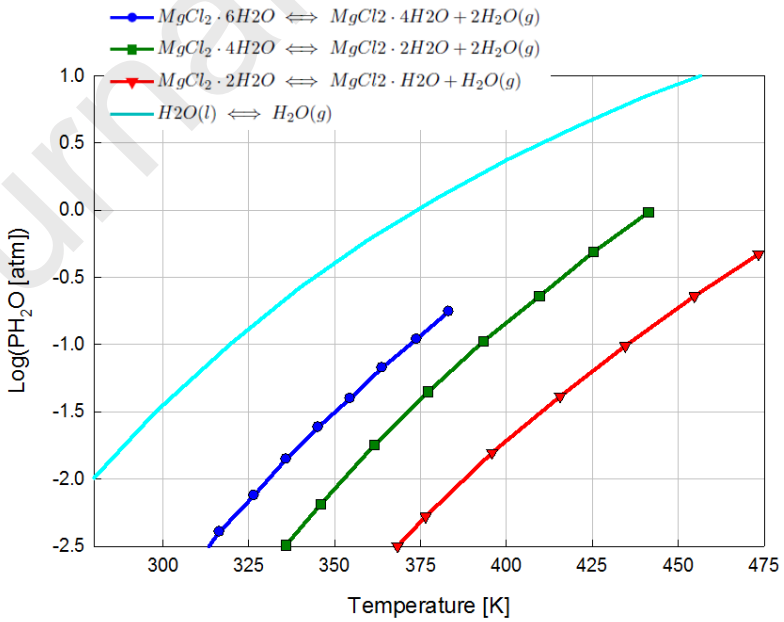

Figure 3: Magnesium chloride hexahydrate equilibrium curve in a psychometric chart [26].

2.1.5 Reaction Kinetics

The activation energy of magnesium chloride hydrate equals 70.4 kJ/mol and it is the most important kinetic parameters of salt hydrate which describes the strengths of the chemical bonds. The reaction rate for dehydration is represented by [47];

$$r_w = -C_a \exp(-\frac{E_a}{RT_s})(\frac{P_F - P_{eq}}{P_{eq}}) \quad (14)$$

where E_a, P_f, P_{eq} and C_a are the activation energy, fluid pressure, equivalent pressure, and pre-exponential constant, respectively.

2.1.6 Heat of Reaction

The heat of reaction for Magnesium chloride is reported in Table 3 as a function of the temperature [26].

Table 3: Heat of reaction for desorption of magnesium chloride hydrates.

Material	Reaction	$\Delta H = A+BT+CT^2$ (KJ/kg H_2O)		
		A	B	C
Magnesium Chloride	$MgCl_2.6H_2O \Leftrightarrow MgCl_2.4H_2O + 2H_2O_{gas}$	3229.7	0.1939	$-6.4548*10^{-4}$
	$MgCl_2.4H_2O \Leftrightarrow MgCl_2.2H_2O + 2H_2O_{gas}$	3831.1	0.0348	$-6.4548*10^{-4}$

2.2 Numerical Solution

COMSOL Multiphysics Modeling Software 5.2 is used to develop the numerical solution of the current open system mathematical model. The main items used in the software are; Brinkman equations, heat transfer in porous media, transport of diluted species in porous media, chemistry and Multiphysics. The validation of the numerical solution is carried out by the experimental results of Rubino and Boer [26] and Marias et al. [25] for the same conditions and input parameters. Figure 4 shows a comparison for the bed temperature at a height of 7.5 cm and radius of 14 cm between the present numerical results and the experimental results of Rubino and Boer [26]. Figure 5 indicates that the present model predicts well the experimental results and the maximum deviation between the two results is about 7%. Figure 5 displays a comparison between the recent simulation results and experimental results of Marias et al. [25] for the bed outlet temperature during charging test using Aluminum potassium sulfate 12-hydrate for the same conditions, such as pressure, volume flow rate and inlet temperature used in the experimental work.

The air temperature at the reactor inlet was 65°C, the humidity for indoor air was absolute humidity and the flow rate was 150 m^3/h. It is noticed from the figure that there is a reasonable agreement between the present model results and the experimental ones, and the maximum relative error is about 8% at the end of the dehydration test.

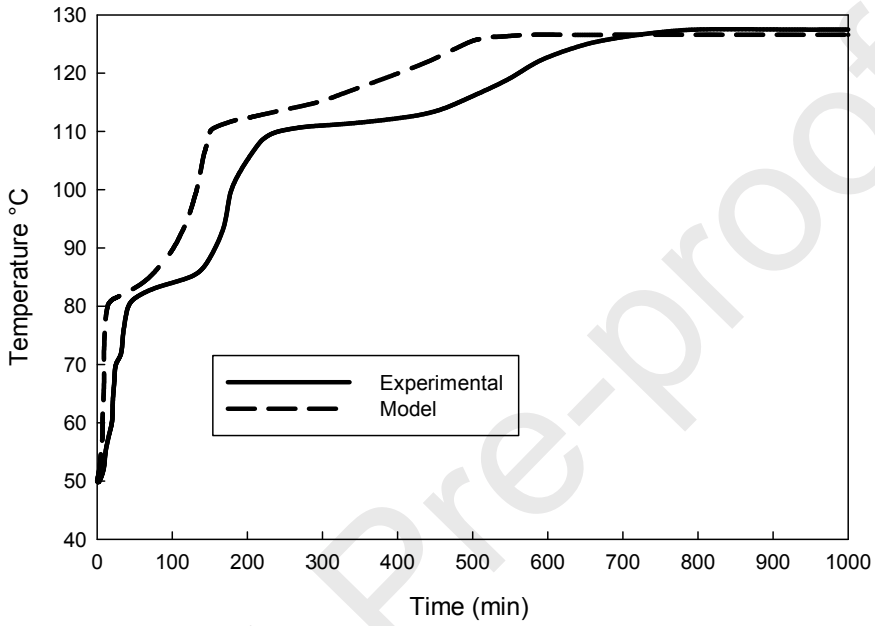

Figure 4: Comparison between the present model results and experimental data of Rubino and Boer [26].

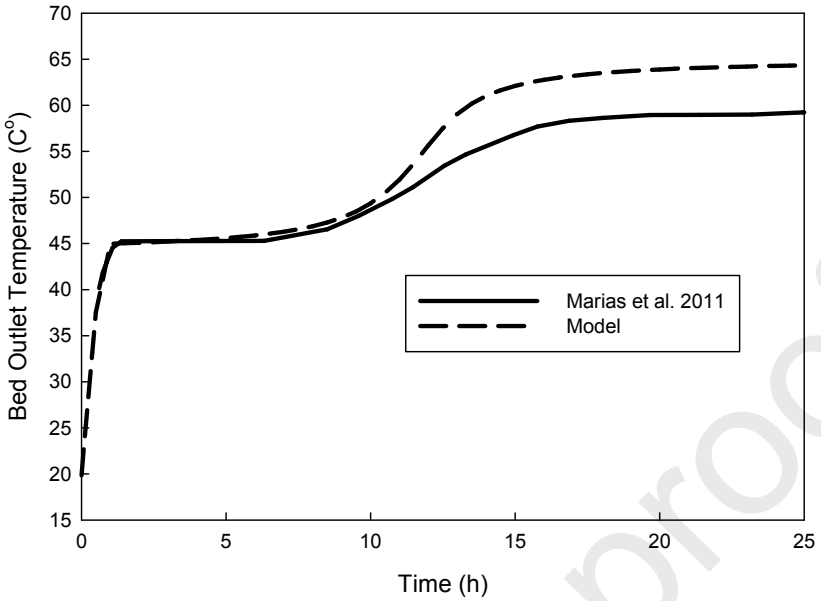

Figure 5: Variation of the bed outlet temperature of the present model and experiment results of Marias et al. [25].

3. Results and Discussions

In this study, the design of the reactor is changed, especially in the inlet and outlet area of the geometry without any change in the volume and height of the reactor. Two shapes of the reactor are considered; cylindrical (case 1 of AR=1) and truncated cone of divergent AR of 1.4 (case2), 4 (case3), and 5.8 (case 4) and convergent AR of 0.71 (case 5), 0.25 (case 6), and 0.17 (case 7) as stated previously.

3.1 Dehydration Process

The charging process of $MgCl_2.6H_2O$ [24,27,39] starts with air temperature initially at 50 °C entering the reactor. Then, the temperature of inlet air rises gradually at a rate equals 1 [˚C/min] until it reaches 127 °C. It is assumed that the inlet air velocity to each reactor design is constant at 0.1 m/s. The heated air continues flowing through the bed until the porous material ($MgCl_2.6H_2O$) becomes full dehydrated. The dehydration of $MgCl_2.6H_2O$ occurs in two stages. The gradual increase in the rate of inlet air temperature is significantly important to prevent the sudden conversion and agglomeration of the first layer facing the inlet air. Moreover, it is important for $MgCl_2.6H_2O$ materials to absorb enough heat energy to be warm and ready for the chemical reaction. During the dehydration process, the inlet air temperature increases from 50 to 127 ˚C at a rate of 1˚C/min during the dehydration process.

3.2 Impact of Reactor Design

The shape of the reactor will influence the dehydration process because, for example, the nozzle reactor shape accelerates fluid flow velocity with decreasing pressure. While, the diffuser reactor shape slows down the fluid flow with increasing the pressure. In consequence, the heat transfer process between the thermochemical material and the air will change with changing the reactor design. Moreover, changing the cross-sectional area of the reactor (diffuser, or nozzle compared to cylinder), varies the quantity of the thermochemical material exposed to air through the reactor length which affects for example on the vapor release rate from the material to the air, etc. Hence, the impact of the reactor design on the air mass flow rate, temperature difference, pressure difference, concentration, and storage energy is studied.

3.2.1 Air Mass Flow Rate

A comparison of the dehydration of $MgCl_2.6H_2O$ is carried out for the different reactor designs of the same volume and dehydration period (2000 min). Figure 6 displays the mass flow rate of the air through the calcium chloride hydrate for the seven designs. Overall, the airflow rate decreases gradually at the beginning of the dehydration process and then will be constant as shown in figure 6 because the inlet temperature increases at the same time until 127 ˚C. Based on the assumed inlet velocity to each reactor design, it is found that the airflow rate of the cylindrical reactor is about 30 kg/h and it intermediates the airflow rate values of the seven cases as stated in Figure 6. Nonetheless, the mass flow rate of case 4 (AR= 5.8) is the highest around 49 kg/h and the least value occurs in case 7 (AR=0.17) which is about 8 kg/h.

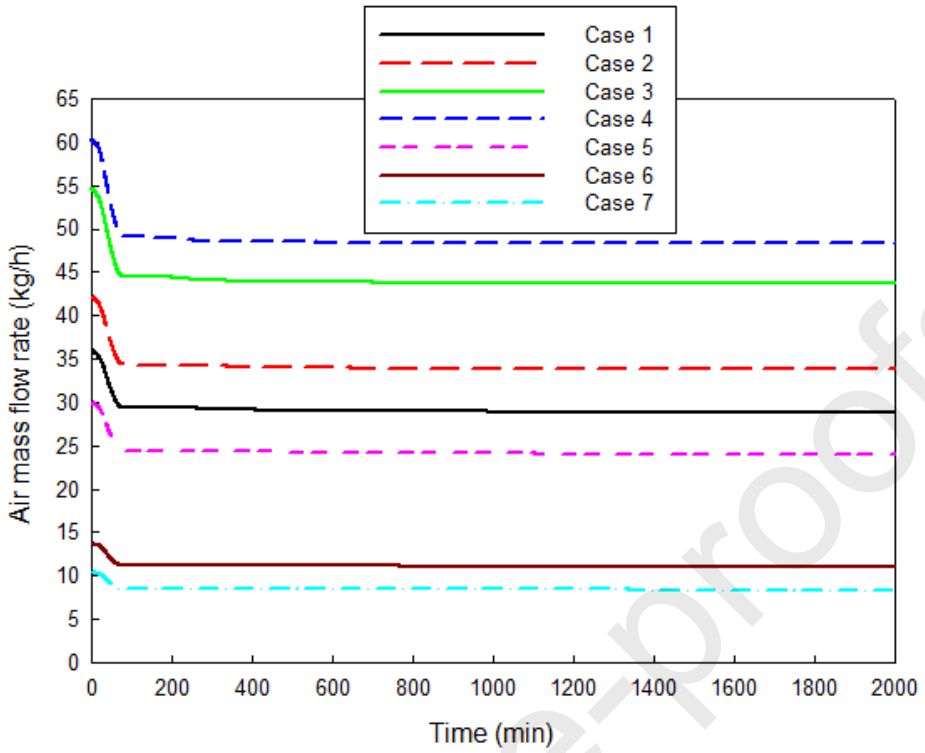

Figure 6: Variation of the mass flow rate of air through salt hydrate with time.

3.2.2 Temperature Difference

Due to the difficulty of representing sometimes the seven cases on the same graph, cases 2, 3 and 4 are compared to case1, and then cases 5, 6 and 7 are compared to case 1 also. Figure 7a shows a comparison between cases 1, 2, 3 and 4 related to the temperature difference between the inlet and outlet air with the operating time for $MgCl_2.6H_2O$. This figure indicates that the reactor design hasn't a sensible effect on the sensible heating of the material. Moreover, it is clear from the figure that the 4th reactor design (case 4) has the lowest dehydration operating time which is about 16 hours, compared with cases 3, 2 and 1which are around 18, 26 and 30 hours, respectively. This indicates that the dehydration rate of the material in case 4 design is greater than the other cases and absorbs less energy to hydrate as will be shown later. Figure 7a shows that cases 4 and 3 are efficient than case 1 and 2 with related to the dehydration time because the dehydration time is considered an important factor when the source of heat is limited by the time as the solar energy applications. From figure 7a results, it is found that as an overall trend, the greater the entrance area compared to the outlet area, the shorter the operating time of charging is required. From the previous results, it can be concluded that by comparing the studied reactor configurations with

respect to diverged truncated cone, the cylindrical shape is not proper design with respect to the dehydration time especially for valuable short time energy like solar energy. Figure 7a also illustrates that case 1 has the maximum temperature difference compared to cases 2, 3 and 4. This means that the lower operating time is the lower temperature difference.

A comparison between cases 5, 6, 7 and 1 related to the temperature difference between the inlet and outlet air with operating time is also illustrated in Figure 7b. This figure demonstrates that the percentage of charging process for a given operating time, as case 1, has the lowest operating time compared with cases 5, 6 and 7 which accords the previous results. While the air enters the reactor and the temperature increases dramatically with a constant rate reaching to a peak at 127 °C. It is significantly seen that cases 6 and 7 require more operating dehydration time for complete desorption process than case 1 where the full dehydration takes place at approximately 16 hours. For cases 5, 6 and 7, the less entrance area, the more operating time is required. Figure 7b illustrates the same previous results as the lower operating time case is the highest temperature difference case. For the divergent cone design, the maximum temperature difference (about 74 ^{o}C at case 7) increases by about 41% compared to the convergent cone design. However, the dehydration time increases more than three times due to change the reactor design from convergent cone to divergent cone of case 7.

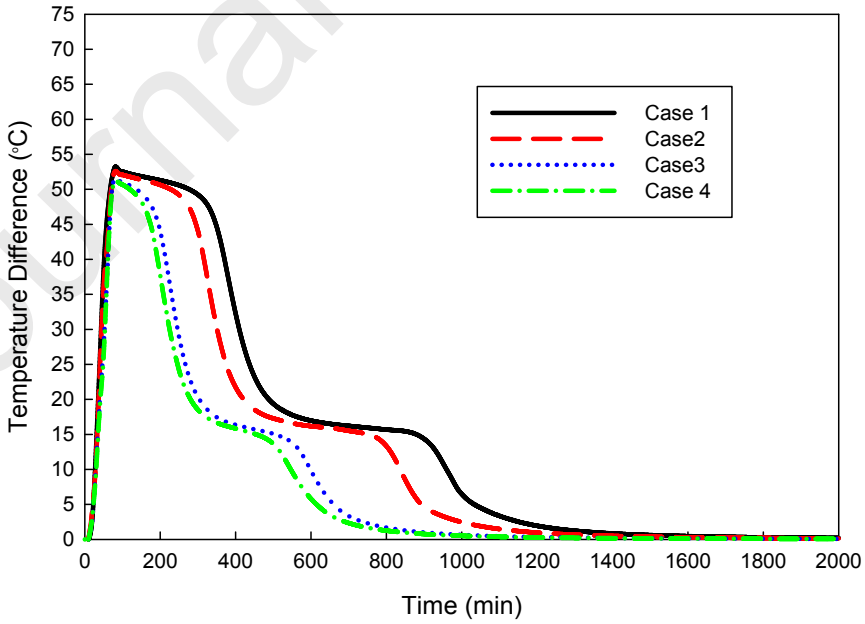

(a) Cases 1, 2, 3 and 4

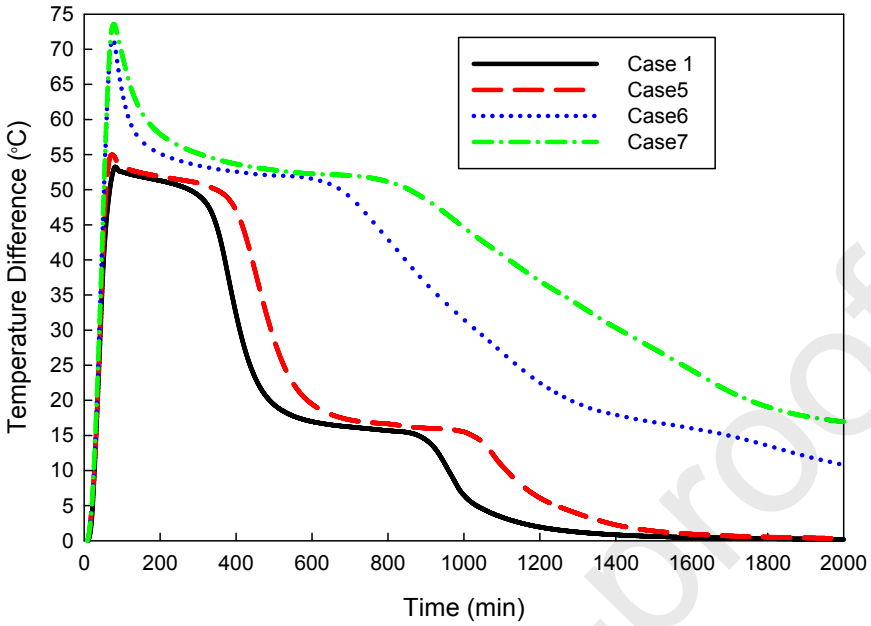

(b) Cases 1, 5, 6 and 7

Figure 7: Air temperature difference variation with time for $MgCl_2.6H_2O$.

3.2.3 Pressure Drop

Figure 8a displays the variation of the pressure drop through the reactor with time during the dehydration processes for cases 1 to 4. It is revealed that the pressure drop increases intensely with the operating time during the desorption because of the decreasing in vapor content inside the porous material which decreases the porosity. It is noted that the pressure drop in the first half along the dehydration time increases with a higher rate than in the second half because the porous material conversion rate is higher at the first half of the dehydration reaction. Moreover, changing the design from case1 to case 4 improves the charging time as stated previously. However, the pressure drop inside the reactor increases. In Figure 8a, the average pressure drop in case 4 is 340 Pa which is more three times than the reference case (case 1) which is 120 Pa. Also, case 3 has a double rate of pressure drop rise than case 2. It means that case 4 is preferred when the time of charging is the foremost key factor in the storage system like solar applications. While case 1 is preferable compared to cases 2, 3 and 4 when the target is decreasing the pressure drop. It is obviously seen that the growth rate of the pressure drop for cases 1, 5, 6 and 7 has the same trend as the previous cases with lower values as plotted in Figure 8b. Furthermore, case 7 records the

lowest pressure drop inside the reactor. It means that a lower fan or blower power is needed to push the air stream inside the reactor in case 7. While, the average pressure drop in case 1 is approximately double more than its value in case 6 and the pressure drop in case 1 is three times more than in cases 6 and 7. However, the development in the pressure drop between cases 5 and 6 is the highest one, there is no significant effect appearing on charging time during dehydration. Thus, the dehydration reaction time in case 5 is approximately equal in case 1. This could be explained as the pressure difference for case 1 is not highly greater than case 5 to delay the dehydration process in case 5 than case 1. The findings demonstrate that the pressure drop increases from about 42 Pa (case 7) to 350 Pa (case 4) (more than 8 times) while the dehydration time changes from about 1000 (case 4) to more than 2000 min (case 7) due to changing the reactor design.

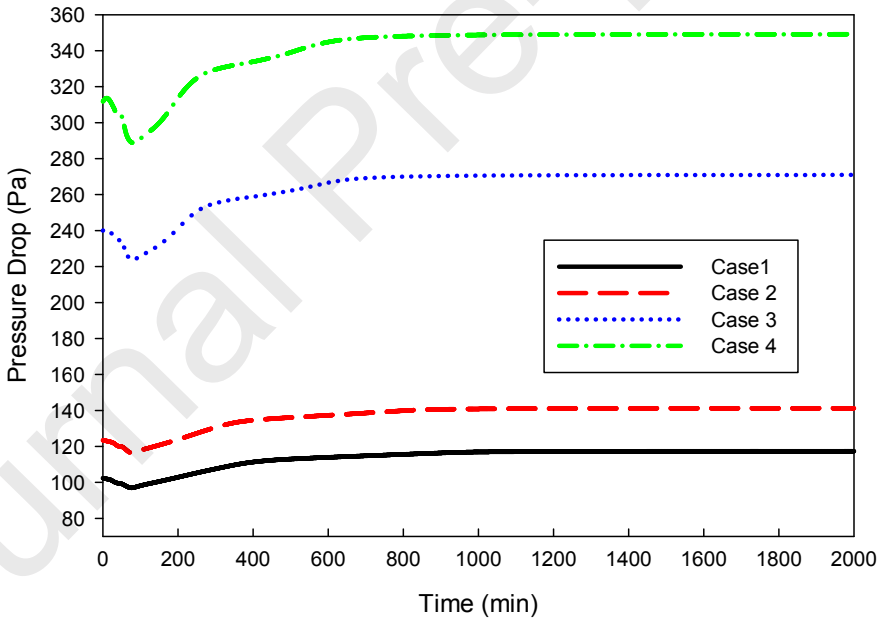

(a) Cases 1, 2, 3 and 4

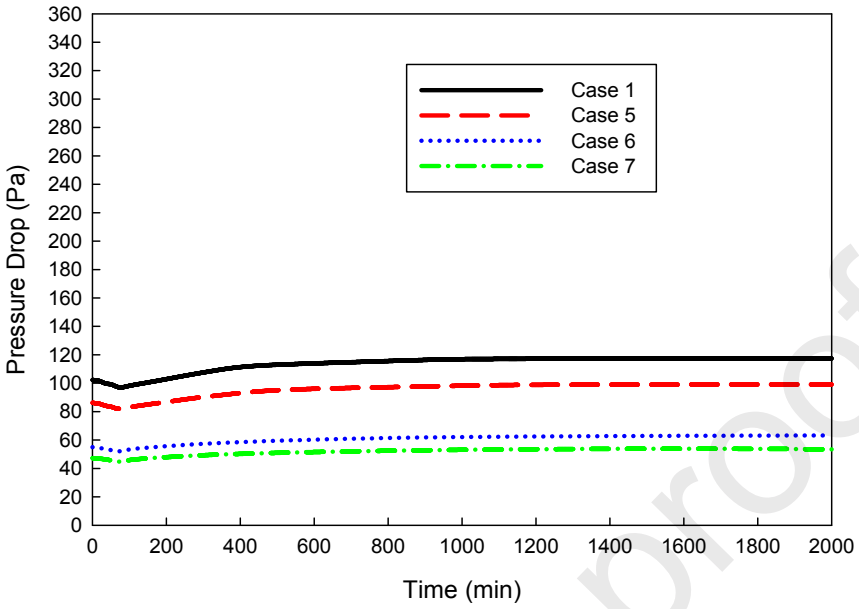

(b) Cases 1, 5, 6 and 7

Figure 8: Pressure drop variation with time for $MgCl_2.6H_2O$.

3.2.4 Concentration

Figure 9 shows the change in the concentration of $MgCl_2.6H_2O$, $MgCl_2.4H_2O$, and $MgCl_2.2H_2O$, respectively with time during the dehydration processes for all studied reactor designs. Overall, the variation of the concentration trend with time of the six design reactors (cases 2 to 7) is the same of the cylindrical reactor (case 1). It is found that the fraction of $MgCl_2.6H_2O$ decreases sharply from about 4400 mol/m^3 close to zero. It is shown that the $MgCl_2.6H_2O$ concentration for case 4 decreases with the highest rate compared to other cases at the beginning of the charging process as stated in Figure 9a. It means that the largest the entrance area, the highest the decreasing rate for $MgCl_2.6H_2O$ and the shorter charging time as stated previously due to changing the reactor shape as mentioned before. Figure 9b shows that the concentration of $MgCl_2.4H_2O$ increases from zero to about 4000 mol/m^3 and then decreases to zero again. The time required for $MgCl_2.4H_2O$ concentration to reach the maximum and to reduce back to the starting fraction is the smallest in case 4 which is about 500 min and it is the longest in case 7 which is 800 min. It is noted that the peak of $MgCl_2.4H_2O$ concentration in case 4 takes place when the $MgCl_2.4H_2O$ concentration starts to rise in case 7. It is found that case 1 intermediates the seven

cases where the convergent cone has the highest concentration while the divergent cone has the lowest concentration. The maximum time required for reaching the maximum complete concentration of $MgCl_2.4H_2O$ for the seven cases is about 700 minutes as shown in Figure 9b. Figure 9 illustrates that material starts with the maximum concentration of $MgCl_2.6H_2O$ and its concentration decreases with time. At the same time, the concentration of $MgCl_2.4H_2O$ increases with time to reach a maximum value of 4200 mol/m^3, then it reduces with time. However, the concentration of the final product $MgCl_2.2H_2O$ increases with time for the instant of decreasing $MgCl_2.4H_2O$ concentration to reach a maximum value and stays constant until the end of the processing time as shown in Figure 9c. The formation of water vapor in the dehydration reaction of magnesium chloride hexahydrate is illustrated in Figure 10 for the seven studied reactor designs. Figure 10a illustrates the instantaneous variation of the vapor concentration with time, however Figure 10b states the variation of the accumulated water vapor with time. Equation 3 and 4 can discuss it as the water vapor releases from both stages of thermochemical reaction and $MgCl_2.2H_2O$ is produced from dehydrated of $MgCl_2.4H_2O$ in one step. It is noted that the reactor design has a significant effect on the concentration of products of magnesium chloride hydrate in the dehydration process. It is found that cases 3 and 4 reach to a maximum vapor concentration faster than other cases while case 7 has the lowest maximum vapor concentration as stated in Figure 10a. Additionally, it is noted that the released vapor increases with time with starting the dehydration process and it drops to zero at the end of the process while the accumulated vapor content increases with time until it reaches to a constant value at the end of the dehydration process as stated in Figure 10.

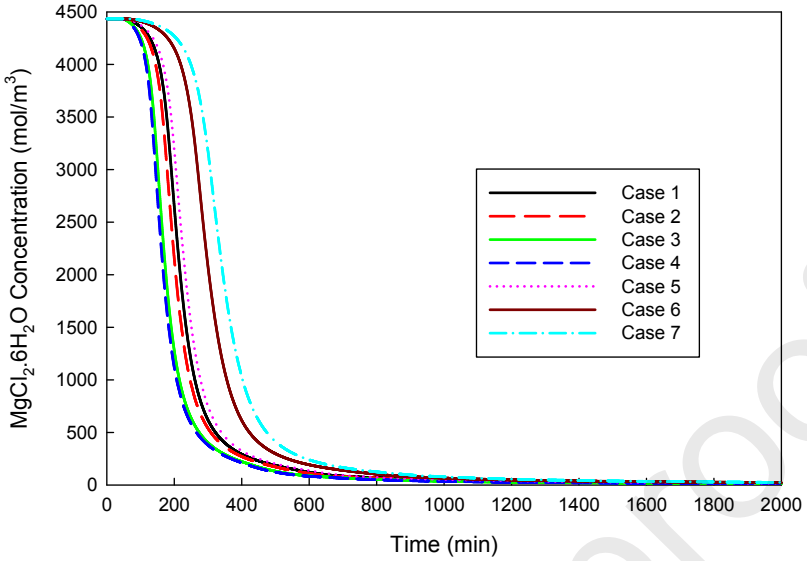

(a) $MgCl_2.6H_2O$.

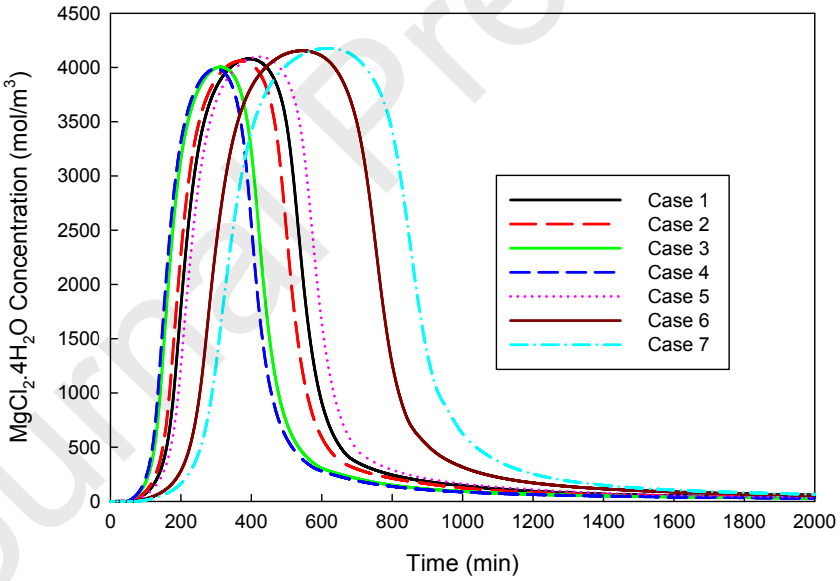

(b) $MgCl_2.4H_2O$.

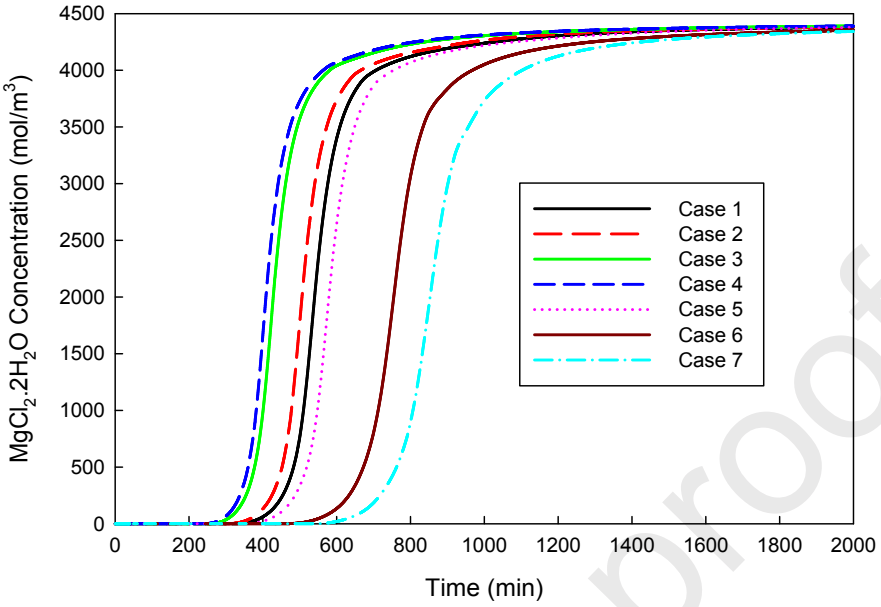

(c) $MgCl_2.2H_2O$

Figure 9: Variation of the concentration with time during the dehydration process.

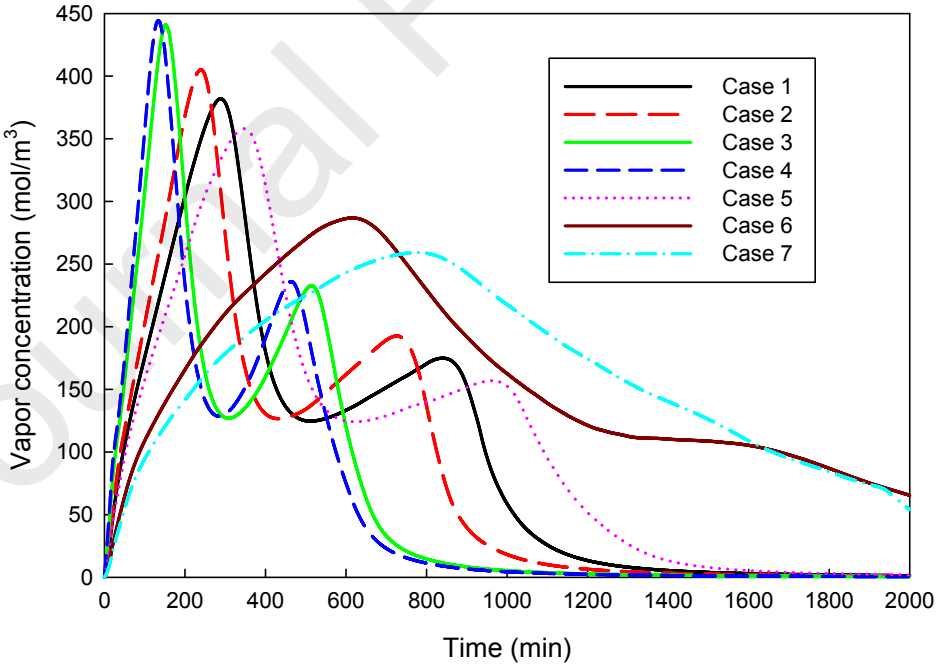

(a)

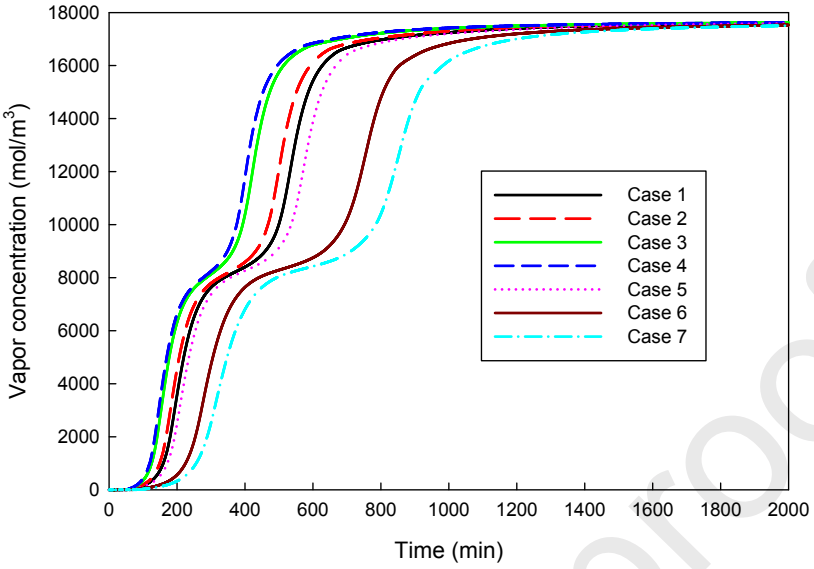

(b)

Figure 10: Variation of the vapor concentration with time (a) instantaneous and (b) accumulated.

3.2.5 Energy Storage

To compare the thermochemical heat storage performance for the seven designs, the integration for the area under the power curve is performed. Figure 11 demonstrates the integration (area under the curve) of the previous power curves for the seven designs. Figure 11 shows that cases 1 and 5 have the highest Thermochemical Heat Storage (THS) and case 7 has the lowest THS. The reason is that in cases 1 and 5, magnesium chloride hydrate reaches the end of reaction at1400 minutes unlike case 7; the salt required more time than 2000 minutes to reach full dehydrated salt. Cases 5 and 2 have thermochemical performance close to case 1 as the change in design is slightly different to that of case 1. However, in cases 3 and 4, the temperature difference reaches zero at 800 minutes and the air mass flow rate is high which shows a bad THS performance. This means that the more time of full dehydration, the more thermochemical heat stored in the salt hydrate. This is due to that the slower desorption process; the hotter air is achived and contacts higher salt materials molecules resulting in an efficient dehydration process. Moreover, the heat stored in case 5 is higher than case 1 with about 66 kJ (increase 0.4%), while the increase of the dehydration time for case 5 compared to case 1 is 16.5%. Consequently, case 5 is the best case as it stored the highest amount of heat. However, from the point of view of the dehydration time, case 4 has a shorter time. Overall, Figure 11 indicates that the maximum

variation of the energy storage of the thermochemical material is about 25.5% due to the variation of the reactor design which signifies that the reactor design can upgrade or downgrade the thermochemical energy storage up to 25.5%. Moreover, the dehydration time can be reduced or increased to more than three times due to the design reactor changing. Maximum stored energy is achieved for the reactor truncated cone of AR 1.4 while the minimum desorption time is obtained for the cone of AR 0.17%.

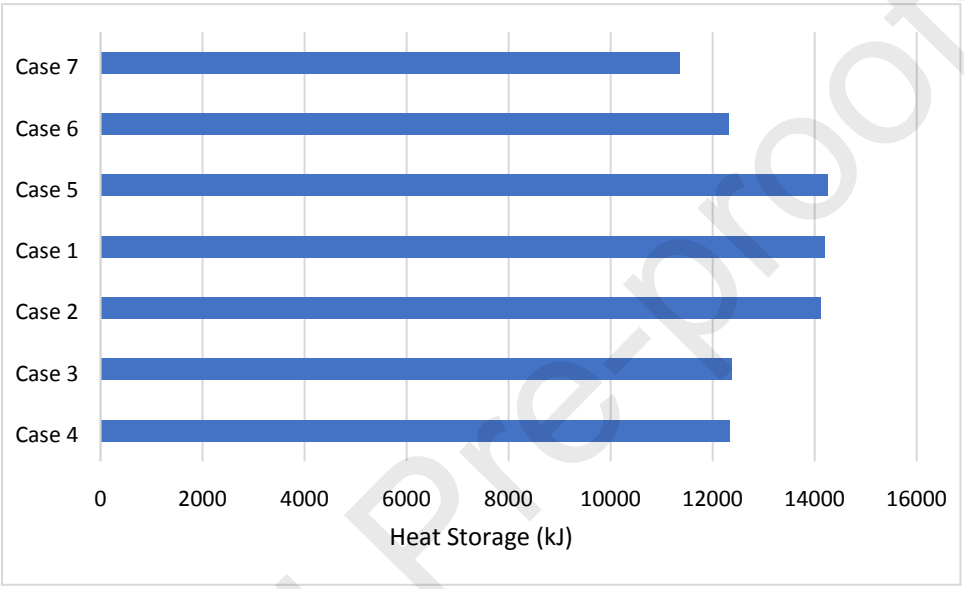

Figure 11: Total thermochemical energy storage in magnesium chloride hydrate for different reactor designs.

4. Conclusion

The impact of the reactor design on the dehydration process for magnesium chloride hexahydrate is studied for inlet air to the reactor heated steadily from 50 to 127 ˚C at a rate of 1 ˚C /min. Two configurations of the reactor design; cylindrical and truncated cone of divergent AR of 1.4, 4 and 5.8, and convergent AR of 0.71, 0.25 and 0.17 are considered during this study. The model of an open thermochemical reactor system for seasonal heat storage is built and investigated using COMSOL Multiphysics Modeling software. The result shows that the dehydration of magnesium chloride hexahydrate takes place in two stages. The variation of $MgCl_2.6H_2O$ concentration is inversely proportional to $MgCl_2.4H_2O$ and in the same manner of the concentrations of $MgCl_2.2H_2O$. However, the concentration of vapor increases steeply with increasing the dehydration time. The smaller area ratio between the outlet and inlet (AR), the

shorter operating time of the dehydration process is required, and the more pressure drop and higher temperature difference are found in the reactor. Consequently, case 4 (AR =5.8) has the lowest dehydration operating time of 16 hours and the highest pressure drop of 340 Pa which is more than seven times of case 7 (AR=0.17). The reactor design hasn't a great effect on the maximum value of the water concentration inside the material during the dehydration process. The most of charging thermal energy inside the material occurs before 800 minutes for cases 2, 3 and 4 compared with 1200 minutes for cases 1 and 5 and 2000 minutes for cases 6 and 7. However, cases 1, 2 (AR =1.4) and 5 (AR=0.71) have the highest Thermochemical Heat Storage (THS) and case 7 has the lowest THS.

ACKNOWLEDGMENT

It is a pleasure to acknowledge the Ministry of Higher Education (MoHE) of Egypt for providing a scholarship to conduct this study as well as the Egypt Japan University of Science and Technology (E-JUST) and Japan International Cooperation Agency (JICA) for offering the facility, tools, and equipment needed to conduct this research work.

Reference

[1] S.H. Osman, Overview of the Electricity Sector in Eqyot, Mediterr. Energy Regul. (2015).

[2] R. Yin, P. Xu, P. Shen, Case study: Energy savings from solar window film in two commercial buildings in Shanghai, Energy Build. 45 (2012) 132–140. doi:10.1016/j.enbuild.2011.10.062.

[3] R. Elghamry, H. Hassan, Impact of window parameters on the building envelope on the thermal comfort, energy consumption and cost and environment, Int. J. Vent. 0 (2019) 1–27. doi:10.1080/14733315.2019.1665784.

[4] R. Parameshwaran, S. Kalaiselvam, S. Harikrishnan, A. Elayaperumal, Sustainable thermal energy storage technologies for buildings: A review, Renew. Sustain. Energy Rev. 16 (2012) 2394–2433. doi:10.1016/j.rser.2012.01.058.

[5] M.S. Yousef, H. Hassan, Assessment of different passive solar stills via exergoeconomic , exergoenvironmental , and exergoenviroeconomic approaches : A comparative study, Sol. Energy. 182 (2019) 316–331. doi:10.1016/j.solener.2019.02.042.

[6] L. K. Edem Liu, N'Tsoukpoe, Hui Le Pierrs, Nolwenn Luo, A review on long-term sorption solar energy storage, Renew. Sustain. Energy Rev. 13 (2009) 2385–2396. doi:10.1016/j.rser.2009.05.008.

[7] P. Pinel, C.A. Cruickshank, I. Beausoleil-Morrison, A. Wills, A review of available methods for seasonal storage of solar thermal energy in residential applications, Renew. Sustain. Energy Rev. 15 (2011) 3341–3359. doi:10.1016/j.rser.2011.04.013.

[8] P. Tatsidjodoung, N. Le Pierrès, L. Luo, A review of potential materials for thermal

energy storage in building applications, Renew. Sustain. Energy Rev. 18 (2013) 327–349. doi:10.1016/j.rser.2012.10.025.

[9] M.A. Said, H. Hassan, Effect of using nanoparticles on the performance of thermal energy storage of phase change material coupled with air-conditioning unit, Energy Convers. Manag. 171 (2018) 903–916. doi:10.1016/j.enconman.2018.06.051.

[10] B. Michel, P. Neveu, N. Mazet, Comparison of closed and open thermochemical processes, for long-term thermal energy storage applications, Energy. 72 (2014) 702–716. doi:10.1016/j.energy.2014.05.097.

[11] B. Wu, H. Ma, Z. Pan, J. Wang, W. Qu, B. Wang, Drying and quality characteristics and models of carrot slices under catalytic infrared heating, Int. Agric. Eng. J. 23 (2014) 70–79. doi:10.1002/er.

[12] A.A. Hawwash, H. Hassan, M. Ahmed, S. Ookawara, K. El Feky, Long-term Thermal Energy Storage Using Thermochemical Materials, Energy Procedia. 141 (2017) 310–314. doi:10.1016/j.egypro.2017.11.111.

[13] A.E. Kalyva, E.C. Vagia, A.G. Konstandopoulos, A.R. Srinivasa, A. T-Raissi, N. Muradov, K.E. Kakosimos, Hybrid photo-thermal sulfur-ammonia water splitting cycle: Thermodynamic analysis of the thermochemical steps, Int. J. Hydrogen Energy. 42 (2017) 9533–9544. doi:10.1016/j.ijhydene.2017.01.104.

[14] J. Lu, Y. Chen, J. Ding, W. Wang, High temperature energy storage performances of methane reforming with carbon dioxide in a tubular packed reactor, Appl. Energy. 162 (2016) 1473–1482. doi:10.1016/j.apenergy.2015.03.140.

[15] S. Tescari, C. Agrafiotis, S. Breuer, L. De Oliveira, M. Neises-Von Puttkamer, M. Roeb, C. Sattler, Thermochemical solar energy storage via redox oxides: Materials and reactor/heat exchanger concepts, Energy Procedia. 49 (2013) 1034–1043. doi:10.1016/j.egypro.2014.03.111.

[16] Y. Kato, T. O-shima, Y. Yoshizawa, Thermal performance of a packed bed reactor for a high-temperature chemical heat pump, Int. J. Energy Res. 25 (2001) 577–589. doi:10.1002/er.704.

[17] M. Jin, P. Frohberg, Y. Sun, P. Li, J. Yu, J. Ulrich, Study on metastable zone width and crystal growth of a ternary system: Case study MgCl2·6H2O·1,4-dioxane, Chem. Eng. Sci. 133 (2014) 181–189. doi:10.1016/j.ces.2014.12.025.

[18] Y. Yoshizawa, KINETIC STUDY OF THE HYDRATION OF MAGNESIUM OXIDE FOR A CHEMICAL HEAT PUMP Yukitaka Kato ,* t Norimichi Yamashita ,: ~ Kei Kobayashi : ~ and, Appl. Therm. Eng. 16 (1996) 853–862.

[19] F. Schaube, L. Koch, A. Wörner, H. Müller-Steinhagen, A thermodynamic and kinetic study of the de- and rehydration of Ca(OH)2at high H2O partial pressures for thermo-chemical heat storage, Thermochim. Acta. 538 (2012) 9–20. doi:10.1016/j.tca.2012.03.003.

[20] G. Balasubramanian, M. Ghommem, M.R. Hajj, W.P. Wong, J.A. Tomlin, I.K. Puri, Modeling of thermochemical energy storage by salt hydrates, Int. J. Heat Mass Transf. 53

(2010) 5700–5706. doi:10.1016/j.ijheatmasstransfer.2010.08.012.

[21] P. Pardo, A. Deydier, Z. Anxionnaz-Minvielle, S. Rougé, M. Cabassud, P. Cognet, A review on high temperature thermochemical heat energy storage, Renew. Sustain. Energy Rev. 32 (2014) 591–610. doi:10.1016/j.rser.2013.12.014.

[22] D. Aydin, S.P. Casey, S. Riffat, The latest advancements on thermochemical heat storage systems, Renew. Sustain. Energy Rev. 41 (2015) 356–367. doi:10.1016/j.rser.2014.08.054.

[23] P.A.J. Donkers, L.C. Sögütoglu, H.P. Huinink, H.R. Fischer, O.C.G. Adan, A review of salt hydrates for seasonal heat storage in domestic applications, Appl. Energy. 199 (2017) 45–68. doi:10.1016/j.apenergy.2017.04.080.

[24] H. a Zondag, V.M. van Essen, L.P.J. Bleijendaal, B.W.J. Kikkert, M. Bakker, Application of MgCl2· 6H2O for thermochemical seasonal solar heat storage, 5th IRES Conf. (2010) 22–24.

[25] F. Marias, G. Tanguy, J. Wyttenbach, S. Rouge, P. Papillon, Thermochemical storage: first results of pilot storage with moist air, Ises Sol. World Congr. - Rapid Transistion to a Renew. Energy World. (2011) 1809–1820. doi:10.18086/swc.2011.29.17.

[26] A. Rubino, R. de Boer, Seasonal Storage of Solar Heat reactor modelling, 10th IIR Gustav Lorentzen Conf. Nat. Refrig. (2012) 1–8.

[27] F. Marias, P. Neveu, G. Tanguy, P. Papillon, Thermodynamic analysis and experimental study of solid/gas reactor operating in open mode, Energy. 66 (2014) 757–765. doi:10.1016/j.energy.2014.01.101.

[28] A.F. Lele, T. Rönnebeck, C. Rohde, T. Schmidt, F. Kuznik, W.K.L. Ruck, Modelling of heat exchangers based on thermochemical material for solar heat storage systems, Energy Procedia. 61 (2014) 2809–2813. doi:10.1016/j.egypro.2014.12.284.

[29] A. Fopah Lele, F. Kuznik, H.U. Rammelberg, T. Schmidt, W.K.L. Ruck, Thermal decomposition kinetic of salt hydrates for heat storage systems, Appl. Energy. 154 (2015) 447–458. doi:10.1016/j.apenergy.2015.02.011.

[30] A. Fopah-Lele, C. Rohde, K. Neumann, T. Tietjen, T. Rönnebeck, K.E. N'Tsoukpoe, T. Osterland, O. Opel, W.K.L. Ruck, Lab-scale experiment of a closed thermochemical heat storage system including honeycomb heat exchanger, Energy. 114 (2016) 225–238. doi:10.1016/j.energy.2016.08.009.

[31] A. Fopah-Lele, F. Kuznik, T. Osterland, W.K.L. Ruck, Thermal synthesis of a thermochemical heat storage with heat exchanger optimization, Appl. Therm. Eng. 101 (2016) 669–677. doi:10.1016/j.applthermaleng.2015.12.103.

[32] T. Yan, C.Y. Wang, D. Li, Performance analysis of a solid-gas thermochemical composite sorption system for thermal energy storage and energy upgrade, Appl. Therm. Eng. 150 (2019) 512–521. doi:10.1016/j.applthermaleng.2019.01.004.

[33] S.A.N. A.A. Hawwash, Ali K. Abdel-Rahman, S. Ookawara, Experimental Study of Alumina Nanofluids Effects on Thermal Performance Efficiency of Flat Plate Solar

Collectors, Int. J. Eng. Technol. 4 (2016) 123–131. doi:10.5176/2251-189X.

[34] A.A. Hawwash, A.K. Abdel Rahman, S.A. Nada, S. Ookawara, Numerical Investigation and Experimental Verification of Performance Enhancement of Flat Plate Solar Collector Using Nanofluids, Appl. Therm. Eng. 130 (2018) 363–374. doi:10.1016/j.applthermaleng.2017.11.027.

[35] R. Olives, S. Mauran, A highly conductive porous medium for solid-gas reactions: Effect of the dispersed phase on the thermal tortuosity, Transp. Porous Media. 43 (2001) 377–394. doi:10.1023/A:1010780623891.

[36] V. Mamani, A. Gutiérrez, S. Ushak, Development of low-cost inorganic salt hydrate as a thermochemical energy storage material, Sol. Energy Mater. Sol. Cells. 176 (2018) 346–356. doi:10.1016/j.solmat.2017.10.021.

[37] A.A. Hawwash, S. Mori, K. El Feky, H. Hassan, Numerical Study for Open Reactor Design Using Salt Hydrate, IOP Conf. Ser. Earth Environ. Sci. 322 (2019). doi:10.1088/1755-1315/322/1/012021.

[38] A. Fopah Lele, F. Kuznik, O. Opel, W.K.L. Ruck, Performance analysis of a thermochemical based heat storage as an addition to cogeneration systems, Energy Convers. Manag. 106 (2015) 1327–1344. doi:10.1016/j.enconman.2015.10.068.

[39] M. Richter, E.M. Habermann, E. Siebecke, M. Linder, A systematic screening of salt hydrates as materials for a thermochemical heat transformer, Thermochim. Acta. 659 (2018) 136–150. doi:10.1016/j.tca.2017.06.011.

[40] G. Tanguy, F. Marias, S. Rouge, J. Wyttenbach, P. Papillon, Parametric studies of thermochemical processes for seasonal storage, Energy Procedia. 30 (2012) 388–394. doi:10.1016/j.egypro.2012.11.046.

[41] H.U. Rammelberg, T. Schmidt, W. Ruck, Hydration and dehydration of salt hydrates and hydroxides for thermal energy storage - Kinetics and energy release, Energy Procedia. 30 (2012) 362–369. doi:10.1016/j.egypro.2012.11.043.

[42] W. Chen, W. Li, Y. Zhang, Analysis of thermal deposition of MgCl2·6H2O hydrated salt in the sieve-plate reactor for heat storage, Appl. Therm. Eng. 135 (2018) 95–108. doi:10.1016/j.applthermaleng.2018.02.043.

[43] H. Zondag, M. Van Essen, L. Bleijendaal, J. Cot, W. Van Helden, W. Planje, T. Epema, H. Oversloot, Comparison of reactor concepts for thermochemical storage of solar heat, Energy. (2008).

[44] C.C.M. Rindt, S.V. Gaastra-Nedea, Modeling thermochemical reactions in thermal energy storage systems, Woodhead Publishing Limited, 2015. doi:10.1533/9781782420965.3.375.

[45] D.A. Nield, A. Bejan, Convection in porous media, 4th ed., Springer, 2013. doi:10.1007/978-1-4614-5541-7.

[46] B. Michel, N. Mazet, S. Mauran, D. Stitou, J. Xu, Thermochemical process for seasonal storage of solar energy: Characterization and modeling of a high density reactive bed,

Energy. 47 (2012) 553–563. doi:10.1016/j.energy.2012.09.029.

[47] M. Lebrun, B. Spinner, Models of heat and mass transfers in solid-gas reactors used as chemical heat pumps, Chem. Eng. Sci. 45 (1990) 1743–1753. doi:10.1016/0009-2509(90)87052-T.

Highlights

- Reducing reactor area ratio, increases pressure drop and decreases charging time.
- Decreasing the outlet to inlet area ratio, reduces the required dehydration time.
- Reactor design hasn't great impact on the maximum value of water concentration.
- Best selection of reactor design rises thermochemical energy storage by 25.5%.
- Increasing full dehydration time, rises thermochemical heat stored in salt hydrate

Author Contribution Statement

The work is a result of the working Ph.D student first author under the main supervision of the second author. All authors that have contributed in the work are listed as they appear in the paper authors list. All funding agency or related any funding for this work were stated in the acknowledgment.

- The authors are responsible for ensuring that the descriptions are accurate and agreed by all authors.

  The authors of the paper

We disclose any actual or potential conflict of interest including any financial, personal or other relationships with other people or organizations within three years of beginning the submitted work that could inappropriately influence, or be perceived to influence, this work.

The authors of the article

A.A. Hawwash, Hamdy Hassan, Khalid El feky